Alexander Ihlow and Udo Seiffert

Microscope color image segmentation for resistance analysis of barley cells against powdery mildew

Microscope Color Image Segmentation for Resistance Analysis of Barley Cells against Powdery Mildew

Alexander Ihlow and Udo Seiffert
Institute of Plant Genetics and Crop Plant Research Gatersleben
Pattern Recognition Group
{ihlow, seiffert}@ipk-gatersleben.de

Abstract

This paper addresses applied image segmentation techniques for the detection of dyed objects (transgenic barley cells) in microscope color images. It is shown on exemplary image data that edge detection with Canny's algorithm applied to the hue channel of the HSV color space outperforms both multidimensional edge detection in RGB space as well as color-based pixel classification. This provides a firm basis for a fully automatic high-throughput analysis tool.

1 Introduction and Problem Statement

Image processing applications can gain significant benefit from color as an additional or exclusive feature beside gray level information. Compared to a gray level image, a color image is no longer a scalar valued function $I(x, y)$: $\mathbb{R}^2 \to \mathbb{R}$, but a vector valued function $\mathbf{I}(x, y)$: $\mathbb{R}^2 \to \mathbb{R}^d$, depending on the spatial coordinates x and y, where each picture element (pixel) can be described by, e.g., the contributions of red, green, and blue (RGB) color, $\mathbf{I} = [I_R, I_G, I_B]^T$.

In bioinformatics applied color image processing plays an important role, especially when features of biological experiments are contained in dyed or somehow differently colored objects. The motivation for this paper is to present some preliminary results of a project in which resistance mechanisms of crop plants against powdery mildew are analyzed from the genetical point of view. Biologists are able to "switch on and off" desired genes in randomly chosen barley cells by a genetical transformation procedure. Such genetically transformed cells are marked for later analysis by a color-indicator, which dyes the whole transformed cell greenish blue. The penetration of the powdery mildew fungus into the cell is indicated by the development of haustoriums [1]. See Figure 1 to get an impression of the image data and the haustoriums.

Such images are acquired by an automatic microscope under control of a computer. The microscope slides are mounted on an x-y table, hence, the complete object can be scanned automatically, e.g.,
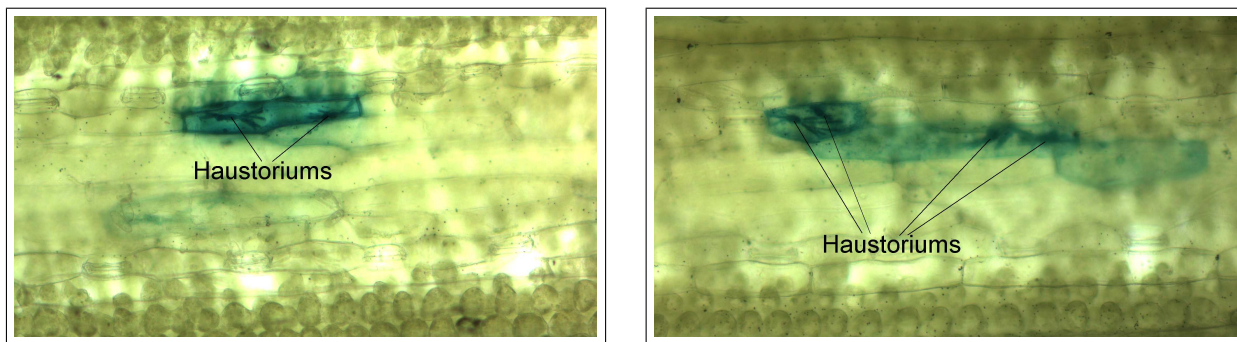

Figure 1: Cutouts of microscope images of barley cells. The greenish dyed ones are genetically transformed and some contain haustoriums of powdery mildew. The original captured images were 2600×2060 pixels, these cutouts are 2000×1100 pixels.

overnight, which produces an enormous amount of image data. Normally, the resolution of an image is 2600×2060 pixels, the displayed images in Figure 1 are cutouts of 2000×1100 pixels. Since there are many potential genes concerning resistance, a huge number of experiments is needed to attain a certain statistical confidence. This motivates firstly the effort on automatic image acquisition hardware and, secondly, the demand for an automatic analysis because manual evaluation is a tedious and time-consuming task for humans. From the present position, two main steps are needed for the automatic analysis: i) Find genetically transformed (dyed) cells and label each cell (image segmentation). ii) Analyze each cell for the development status of haustoriums. This paper deals mainly with the image segmentation procedure and is organized as follows: in Section 2 we evaluate a segmentation approach based on color classification of each pixel using a parametric model for statistical decision making. Section 3 introduces a more advanced and promising technique based on edge detection. Finally, the results are discussed and some conclusions are given in Section 4.

2 Segmentation by Pixel-Color Classification

There is no universal image segmentation algorithm and the literature offers an enormous pool of approaches which work under certain circumstances for a limited class of problems. See, e.g., [2] for an overview about image segmentation. Thresholding a gray-level value is one of the simplest image segmentation techniques. Based on the histogram information, one or more thresholds are calculated and each pixel is assigned to a class. As an extension, a basic approach for *color* image segmentation could be a pixel-wise color classification. Since the information contained in each pixel is no longer a scalar, but a vector (generally the RGB color components), we need a vector-valued analysis technique.
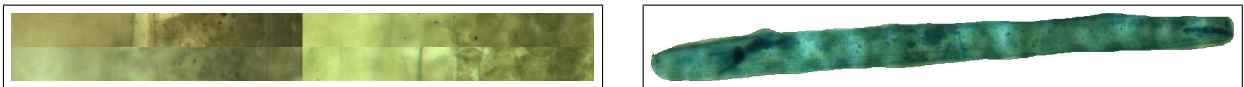

Figure 2: Typical cutouts of *background* (left) and *cell* regions (right).
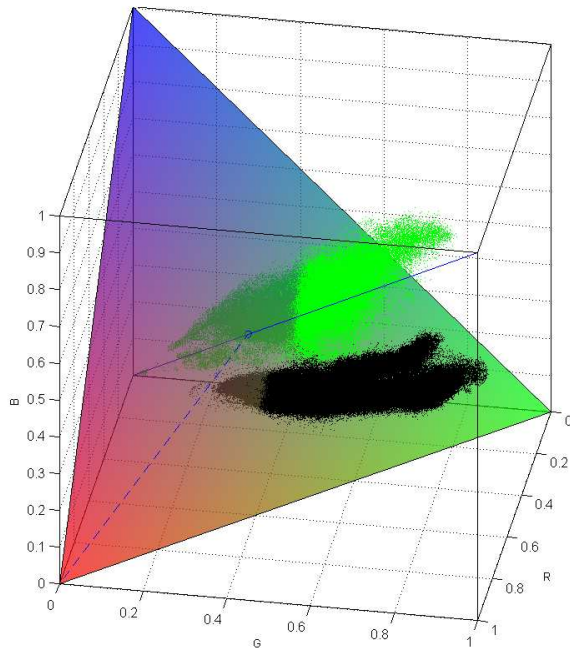

Figure 3: Pixel-color clusters from *background* (black) and *cell* (green) region (compare Figure 2) in RGB space.
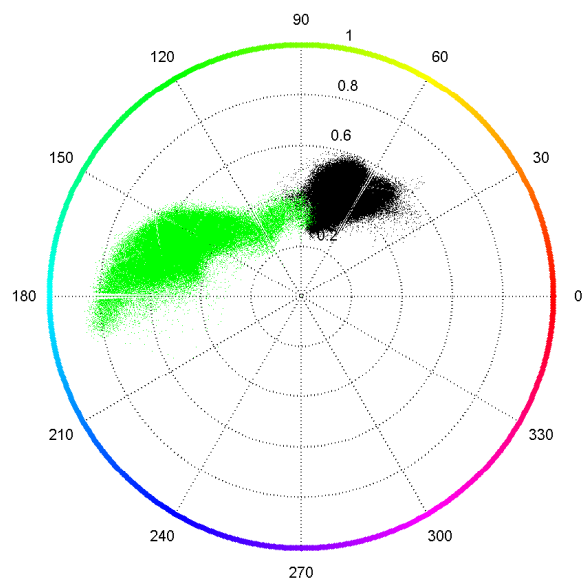
Figure 4: Pixel-color clusters displayed as hue-saturation part of the HSV model. Black is *background*, green is *cell*.

Figure 2 shows two typical cutouts for *background* and *cell* regions of our microscope images, respectively. In Figure 3, the RGB value of each pixel of these *background* and *cell* regions are depicted as black and green dots in 3D while the density of these dots can be interpreted as a 3D histogram. It can be clearly observed that the color of *background* and *cell* regions form two clusters, hence, both regions must be separable somehow. In the next section we will analyze the performance of a Bayesian classification method based on a parametric model of these pixel-color clusters.

2.1 Segmentation in RGB by a Multivariate Gaussian Model Approach

The histogram information contained in these clusters in RGB space (Figure 3) can be approximately described by a parametric model which is used for statistical decision making in the sequel. A both powerful but quite simple model is the Multivariate Gaussian model [3]. Suppose, generally, we have k classes, each with d features. Then, the Multivariate Gaussian model for a class C_i is completely described by the mean vector $\boldsymbol{\mu}_i$ and the covariance matrix $\boldsymbol{\Sigma}_i$

$$\boldsymbol{\mu}_i = \begin{pmatrix} \mu_{i1} \\ \mu_{i2} \\ \vdots \\ \mu_{id} \end{pmatrix}, \quad \boldsymbol{\Sigma}_i = \begin{pmatrix} \sigma_{11}^2 & \sigma_{12}^2 & \cdots & \sigma_{1d}^2 \\ \sigma_{21}^2 & \sigma_{22}^2 & \cdots & \sigma_{2d}^2 \\ \vdots & \vdots & \ddots & \vdots \\ \sigma_{d1}^2 & \sigma_{d2}^2 & \cdots & \sigma_{dd}^2 \end{pmatrix}. \tag{1}$$

This assumes all higher statistical moments than the second one to be zero and approximates the probability density function of class C_i by the Multivariate Gaussian Distribution

$$p(\mathbf{x}|C_i) = \frac{1}{\sqrt{\det \boldsymbol{\Sigma}_i (2\pi)^d}} \exp\left[-\frac{1}{2}(\mathbf{x} - \boldsymbol{\mu}_i)^T \boldsymbol{\Sigma}_i^{-1}(\mathbf{x} - \boldsymbol{\mu}_i)\right], \tag{2}$$

which gives the probability of a sample vector $\mathbf{x}$ to belong to class C_i. The task is now to build this model from representative data of our images, for example from the data according to Figure 3, and to assess the classification performance. Therefore, Bayes' Theorem states that the sample $\mathbf{x}$ should be classified into the class C_i that maximizes

$$P(C_i|\mathbf{x}) = \frac{P(C_i)p(\mathbf{x}|C_i)}{\sum_{j=1}^k P(C_j)p(\mathbf{x}|C_j)}, \tag{3}$$

which is also known as maximum likelihood (ML) classification. $P(C_i)$ is the prior (a priori) probability that a sample belongs to class C_i, and with the knowledge of the probability distributions of each class we calculate the posterior (a posteriori) probability $P(C_i|\mathbf{x})$ given the sample $\mathbf{x}$.

Precisely, our image data is three-dimensional, and the sample vector $\mathbf{x}$ has to be replaced by the vector of the RGB values $[I_R, I_G, I_B]^T$ of each pixel of the image to be segmented.

Furthermore, since we have two classes only (let us call them C_b for *background* and C_c for *cell*), we can easily develop a graphical understanding of the classification process by calculating the optimum decision boundary between the two clusters in RGB space. This decision boundary is given by the quadratic equation (see [3] for derivation)

$$0 = \mathbf{x}^T \mathbf{A} \mathbf{x} + \mathbf{b}^T \mathbf{x} + c, \quad \text{with the parameters} \tag{4}$$

$$\mathbf{A} = \boldsymbol{\Sigma}_c^{-1} - \boldsymbol{\Sigma}_b^{-1} \tag{5}$$

$$\mathbf{b} = -2\boldsymbol{\Sigma}_c^{-1}\boldsymbol{\mu}_c + 2\boldsymbol{\Sigma}_b^{-1}\boldsymbol{\mu}_b \tag{6}$$

$$c = -2\ln(P(C_c)) + 2\ln(P(C_b)) + \ln(\det \boldsymbol{\Sigma}_c) - \ln(\det \boldsymbol{\Sigma}_b) + \boldsymbol{\mu}_c^T \boldsymbol{\Sigma}_c^{-1}\boldsymbol{\mu}_c - \boldsymbol{\mu}_b^T \boldsymbol{\Sigma}_b^{-1}\boldsymbol{\mu}_b, \tag{7}$$

and is either of linear, circular, parabolic, elliptical or hyperbolic character. A linear decision boundery, for example, is obtained when the covariance matrices $\boldsymbol{\Sigma}_b$ and $\boldsymbol{\Sigma}_c$ are equal. Then, the parameter $\mathbf{A}$ gets zero, and the quadratic term in (4) vanishes.

2.2 Validation of the Multivariate Gaussian Model Assumption

How valid is the assumption of a Multivariate Gaussian Distribution to model the pixel-color clusters? We answer this question by inspecting the "Gaussianess" of the decorrelated data of both clusters.

Let a general d-dimensional process be collected from N sample vectors $\mathbf{x}_n \in \mathbb{R}^{d \times 1}$ according to $\mathbf{X} = [\mathbf{x}_1, \mathbf{x}_2, \ldots, \mathbf{x}_N]$. The centered process $\mathbf{X}^{(c)}$ is obtained by subtracting the mean vector $\boldsymbol{\mu}$ of the process from each sample vector, $\mathbf{X}^{(c)} = [\mathbf{x}_1 - \boldsymbol{\mu}, \mathbf{x}_2 - \boldsymbol{\mu}, \ldots, \mathbf{x}_N - \boldsymbol{\mu}]$.

Let $\mathbf{V}_i \boldsymbol{\Lambda}_i \mathbf{V}_i^T = \boldsymbol{\Sigma}_i$ be an eigenvalue decomposition of the covariance matrix of class C_i. Projecting the centered data of class C_i into the space spanned by the eigenvectors of the covariance matrix of class C_i according to

$$\tilde{\mathbf{X}}_i^{(c)} = \mathbf{V}_i^T \mathbf{X}_i^{(c)} \tag{8}$$

decorrelates the data and rotates it such that their principal axis are aligned with the axis of the underlying coordinate system. That principal components of the clusters are displayed in Figure 5, and, as can be clearly seen, they are nearly Gaussian distributed which confirms the validity of the Multivariate Gaussian Model for the considered data.
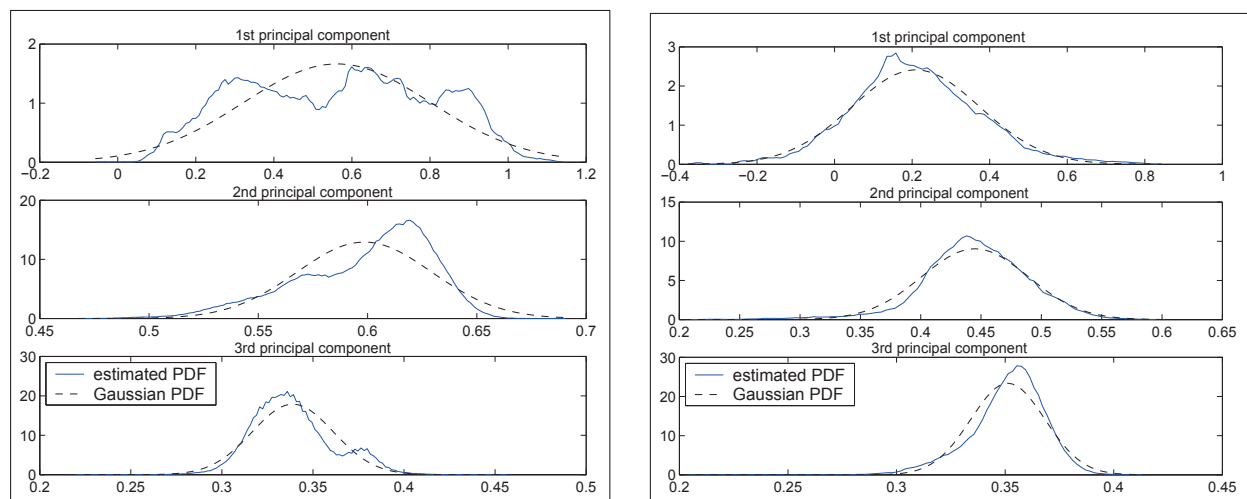

Figure 5: Probability density function (PDF) of the decorrelated RGB-cluster data of *background* (left) and *cell* (right). $\Rightarrow$ The Multivariate Gaussian Model is a good approximation.

2.3 Segmentation Results by Multivariate Gaussian Pixel-Color Classification

Figure 6 shows the segmented images from Figure 1, where every pixel is classified into *background* (white) and *cell* (black). It can be observed that strong-colored cells are marked as a connected region, whereas parts of weak-colored cells appear as fragmented regions. Moreover, the background region is disturbed by several misclassified pixels, but this effect can be removed easily by some morphological post-processing. We conclude at this point that images with isolated strong-colored cells can be labeled by this simple technique, but, since our data is generally not that ideal, we need a more sophisticated and much more reliable technique. From the signal processing point of view, this pixel-color classification method suffers from the *ignorance of all spatial information* of an image and using histogram information only instead. Furthermore, traning data is needed for this classification procedure and variations in our data concerning luminance and color parameters will deteriorate the classification results. These obvious drawbacks are avoided by an edge detection based segmentation approach, as shown in the next section.
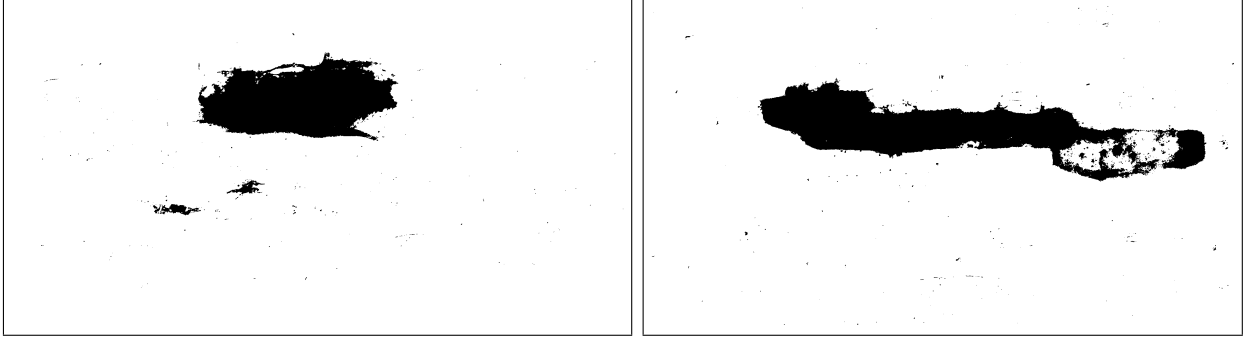
Figure 6: Segmentation into *background* (white) and *cell* (black) by pixel-color classification. ⇒ Weak colored cells are not properly detected.

3 Segmentation by Edge Detection

The ignorance of spatial information leads to a limited image segmentation performance, as concluded in the last section. Edge detection is a powerful approach that inherently exploits spatial information to find salient features in images. An edge detector [4] basicly applies directional derivative operators to an image, e.g., according to linear signal processing as a convolution by an appropriate filter kernel. Depending on this filter and further signal processing, there exists a large number of edge detectors, which can be essentially devided into first-order and second-order derivative based ones. First-order based detectors put a threshold on the gradient image to find potential edge elements (edgels), whereas the latter respond to zero crossings of the second-order derivative. A particularly powerful and prominent edge detector is the one developed by Canny [5]. Its filtering mask is built on a Gaussian derivative with a scale parameter σ, determining the spatial selectivity of the high-pass filter.

$$\frac{\partial I}{\partial x} \approx I * \left(-\frac{x}{\sigma^2} \, \mathrm{e}^{-\frac{x^2+y^2}{2\sigma^2}} \right) \, , \quad \frac{\partial I}{\partial y} \approx I * \left(-\frac{y}{\sigma^2} \, \mathrm{e}^{-\frac{x^2+y^2}{2\sigma^2}} \right) \tag{9}$$

A small scale parameter results in a locally sharp and certain gradient profile while a larger scale parameter reduces false edgels that appear from noisy image data, at the cost of higher uncertainty about the position of edgels. Additionally, a Gaussian low-pass is applied for regularization reasons. Moreover, Canny's algorithm exploits not only the magnitude information $\left(\frac{\partial I}{\partial x}\right)^2 + \left(\frac{\partial I}{\partial y}\right)^2$ of the gradient image, but phase information $\mathrm{atan}\left(\frac{\partial I}{\partial y}/\frac{\partial I}{\partial x}\right)$, too. In connection with a hysteresis thresholding procedure this leads to more connected edges than produced by less advanced edge detectors, and getting *connected* edges is a crucial requirement for our application, since we are looking for relatively large objects that can be described by a closed boundery.

3.1 Multidimensional Edge Detection in RGB

The gradient operations in (9) can only be applied to a scalar valued function, i.e., a gray level image. Now the question arises, how to operate on color images? One approach could be to apply the gradient operation on every vector component independently, as suggested in [6]. In this case, the matrix $\mathbf{S} = \mathbf{J}^T \mathbf{J}$ is build from the Jacobian matrix

$$\mathbf{J} = \left[\begin{array}{ccc} \frac{\partial I_R}{\partial x} & \frac{\partial I_G}{\partial x} & \frac{\partial I_B}{\partial x} \\ \frac{\partial I_R}{\partial y} & \frac{\partial I_G}{\partial y} & \frac{\partial I_B}{\partial y} \end{array} \right]^T \tag{10}$$

and the trace of $\mathbf{S}$ is evaluated as a measure of the joint channel gradient intensity. For the sake of computational complexity, we downsample our images from Figure 1 by a factor of four, hence, we end up in a resolution of 500×275 pixels. From Figure 7 it can be observed that the arising

gradient profile does not represent the salient features of our images, namely the greenish cells, very well, but other unwanted parts are highlighted instead. Intuitively, this is caused by operating on both luminance and color information, whereas the features we are looking for are mainly caused by changes in color and not by changes in brightness. Therefore, we transform the image from RGB space into another color space where brightness and color information are separated and choose the HSV (Hue Saturation Value) color space as an appropriate candidate.
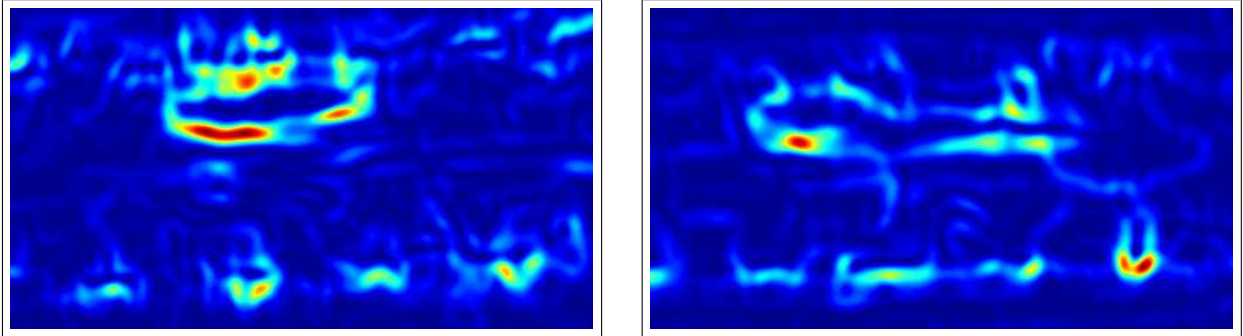

Figure 7: Magnitude of multichannel gradient according to the trace of $\mathbf{S} = \mathbf{J}^T\mathbf{J}$ from Eq. (10). Image size 500×275 pixels, $\sigma = 5$. $\Rightarrow$ The salient features (the greenish cells) do *not* appear clearly.

3.2   Edge Detection in HSV domain

After the transformation of RGB data into HSV (Hue Saturation Value) color space, the data is still three-dimensional, but needs a completely different interpretation than in RGB space. Hue specifies the color and is inherently an angle, i.e., it has a cyclic or periodic character. See again Figure 3 and focus on the color plane with the red green and blue end points. The color angle in HSV is defined to start at red, goes on via green to blue and back to red. This full circle can be mapped onto an axis from zero to one, and red color has both values, zero and one, because of the cyclic character. The distance from the center of the plane is the saturation of a color and states how much the pure color is diluted by white. Last but not least the value channel is related to the equivalent gray level. Since the HSV transform is entirely non-linear, the terms "angle", "distance" and "gray level" have to be treated in the broader sense. See [7] for details on the HSV transformation.
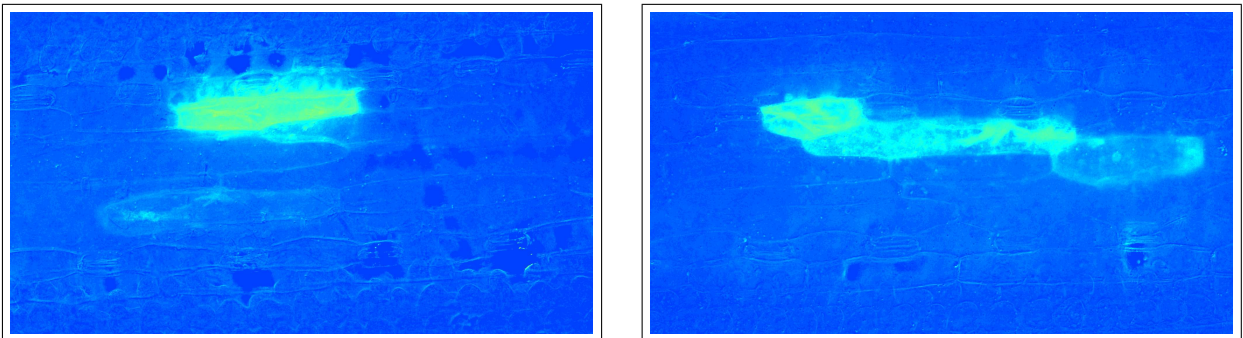

Figure 8: Hue channel in HSV color space of the microscope images from Figure 1.

In Figure 4, the hue-saturation plane of the HSV model is depicted with the corresponding transformed color clusters from Figure 3. The mean hue of the *background* and *cell* cluster are about 60° and 150°, respectively. The hue channel of the images from Figure 1 is depicted miscolored in Figure 8. It can be observed that the hue channel contains mainly the features of our images which we are looking for — thus the hue channel seems to be appropriate for edge detection in a

single color component to find the greenish cells in our images. We note again that hue is not a linear but a periodic axis, and one has to be careful in generalizing edge detection on hue channel. In our case, this is valid because our images contain no red color components which are located around the cyclic ambiguity of the hue axis.
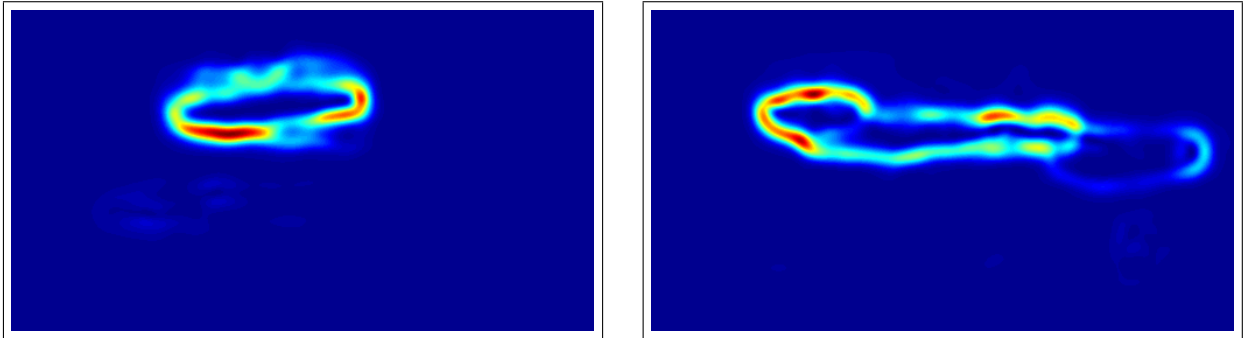

Figure 9: Gradient magnitude image of hue channel. Image size 500×275 pixels, $\sigma = 5$. $\Rightarrow$ The salient features (the greenish cells) appear clearly.

The gradient magnitude profile at a scale of $\sigma = 5$ is depicted in Figure 9. As a result, the object bounderies of our dyed genetically transformed cells are clearly detectable. The resulting edgels are calculated by hysteresis thresholding and overlaid into the original image, as depicted in Figure 10. The result looks promising, the detected edgels belong mainly to the objects we are looking for, but there are also false edgels which have to be removed. Now, intelligent further processing is needed to link the detected edgels together such that each cell can be labeled individually. In fact, simple local neighborhood based edge linking approaches help in some cases to "repair" broken edges but cannot fulfill our high demands on cell detection performance. Recently, a promising edge-linking approach for closed contours was published [8], which may help to generally solve that problem. Another approach to connect true edgels to closed objects is to work on multiple scales. As can be seen in Figure 11, where Canny edge detection was done with a "rigorous" scale of $\sigma = 12$, the region of interest is bordered by a closed boundery. Such closed edges can easily be identified and a subtler analysis can be performed at lower scales, taking the coarse segmentation information from larger scales into account to remove false edgels. This leads to a hierarchical system using different scales of the Canny detector. The goal is to find and mark each individual transformed cell even in cell compounds, like the three connected ones in the second sample image.

4   Conclusions and Future Work

In this paper, we have discussed image segmentation techniques for microscope color images that have to be analyzed automatically in biological research applications and we have demonstrated the segmentation performance on two exemplary images. Simple pixel-based classification methods cannot accomplish the demands on segmentation performance, whereas edge detection on the hue channel of the HSV color space performs very promising on our image data. With Canny's edge detector the region of interest is found as a closed contour, when it is tuned with a large scale parameter σ. Fortunately, the resulting edges are relatively insensitive to changes of the edge detector thresholds, which emphasizes a certain robustness of the used techniques. Some work still needs to be done to separate cell compounds and label each cell individually as well as to check each labeled object to be truely a single genetically transformed cell. This is crucial for the confidence of the resulting statistics.

In the future, the suggested segmentation procedure has to stand the test and we have to go on solving the problem of detecting the development status of haustoriums within the segmented genetically transformed cells to get closer to a pure automatic machine-driven tool that helps analyzing thousands of images.
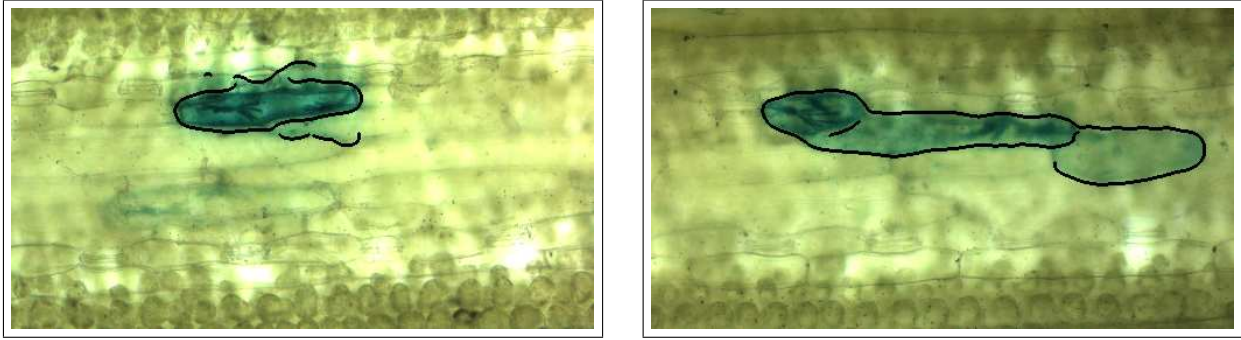
Figure 10: Edgels detected with Canny's algorithm on hue channel with $\sigma = 5$, low threshold 0.16, high threshold 0.40.
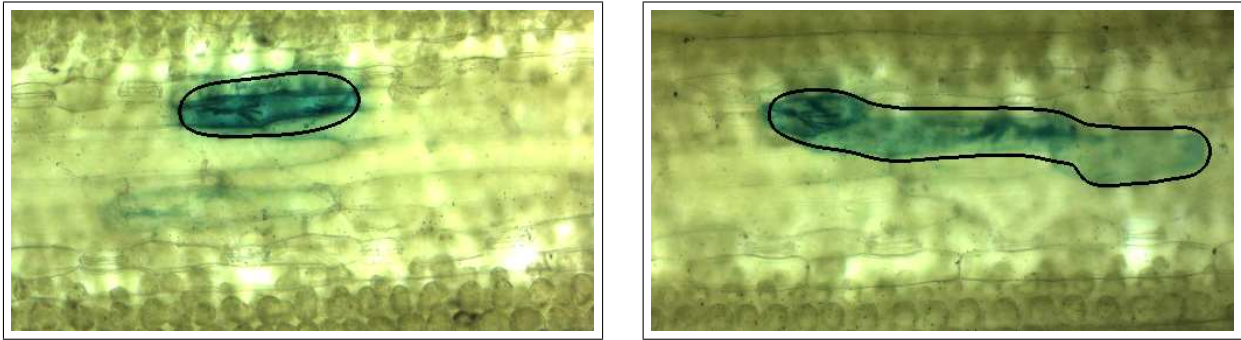

Figure 11: Edgels detected with Canny's algorithm on hue channel with $\sigma = 12$, low threshold 0.16, high threshold 0.40.

References

[1] Patrick Schweizer, Jana Pokorny, Olaf Abderhalden, and Robert Dudler. A transient assay system for the functional assessment of defense-related genes in wheat. *Molecular Plant-Microbe Interactions*, 12(8):647–654, 1999.

[2] Nikhil P. Pal and Sankar K. Pal. A review on image segmentation techniques. *Pattern Recognition*, 26(9):1277–1294, 1993.

[3] Earl Gose, Richard Johnsonbaugh, and Steve Jost. *Pattern Recognition and Image Analysis*. Prentice Hall, 1996.

[4] Djemel Ziou and Salvatore Tabbone. Edge detection techniques – an overview. *International Journal of Pattern Recognition and Image Analysis*, 8:537–559, 1998.

[5] John F. Canny. A computational approach to edge detection. *IEEE Transactions on Pattern Analysis and Machine Intelligence (PAMI)*, 8(6):679–698, November 1986.

[6] Bernd Jähne. *Digitale Bildverarbeitung*. Springer, 2002.

[7] Stephen J. Sangwine, editor. *The Colour Image Processing Handbook*. Chapman & Hall, London, 1st edition, 1998.

[8] Shyjan Mahamud, Lance R. Williams, Karvel K. Thornber, and Kanglin Xu. Segmentation of multiple salient closed contours from real images. *IEEE Transactions on Pattern Analysis and Machine Intelligence (PAMI)*, 25(4):433–444, April 2003.